RSC Advances




ROYAL SOCIETY OF CHEMISTRY

www.rsc.org/advances

# Effect of multi-walled carbon nanotubes on the morphology evolution, conductivity and rheological behaviors of poly(methyl methacrylate)/ poly(styrene-*co*-acrylonitrile) blends during isothermal annealing

Hui-hui Li, Min Zuo,* Ting Liu, Qi Chen, Jifei Zhang and Qiang Zheng

**Abstract**

The effect of multi-walled carbon nanotubes (MWNTs) on the morphological evolution, conductive and viscoelastic behaviors for partially miscible blends of poly (methyl methacrylate)/poly(styrene-*co*-acrylonitrile) (PMMA/SAN) upon annealing above the phase-separation temperatures was investigated via microscopic technology, melt rheology and simultaneous measurement of rheological and conductive properties. The well-dispersed MWNTs in the homogeneous matrix preferentially migrated into the SAN-rich phase after the occurrence of phase separation and then further agglomerated in the SAN-rich phase to form the conductive pathway. The effect of MWNTs on the phase separation temperatures of PMMA/SAN blend was found to depend on the composition of blend matrix, as a result of the composition difference between surface layer of MWNTs and polymer matrix induced by the selective absorption of SAN on the surface of MWNTs. Thermal-induced dynamic percolation was observed for both the resistivity $\rho$ and dynamic storage modulus $G'$ as a function of annealing time. The respective contribution of phase separation and MWNTs aggregation to the variation of $G'$ was also clearly distinguished during annealing. The influence of temperature and filler loading on the percolation time of $\rho$ was investigated and the activation energies of dynamic conductive (DC) percolation were determined, independent on the volume content of MWNTs. The activation energies of DC percolation for the nanocomposites were found to be close to those of viscous flow for SAN.

**Keywords:** Phase separation, Multi-walled carbon nanotubes, Percolation, Rheology, Electrical Conductivity

*MOE Key Laboratory of Macromolecule Synthesis and Functionalization, Ministry of Education, Department of Polymer Science and Engineering, Zhejiang University, Hangzhou 310027, China*

*E-mail: kezuomin@zju.edu.cn

## 1. Introduction

Conductive polymer composites (CPCs) have received considerable interests in the polymer composite research field for their tunable properties and multifunction performances, such as electromagnetic interference (EMI) shielding,[1] sensing, [2] flexible electronics and so on.[3, 4] Typically, through the incorporation of conductive particles into polymer matrix, the CPC materials would be provided with conductive property originating in its conductive network. The conductivity of CPC jumps greatly when the filler content reaches the static electrical percolation threshold ($\rho_c$). In general, more conductive fillers are incorporated into the CPC materials for greater conductivity, but this often causes poor processibility and mechanical properties at the same time. However, building a conductive network within an insulated polymer matrix does not necessarily require a high filler concentration and a well distribution state of filler particles, the conductivity of CPC materials can be also enhanced by controlling the selective distribution of conductive fillers with small loadings.[1]

Incorporating conductive fillers into multiphase polymer blends is considered as a simple but efficient way to obtain the excellent conductivity and reduce the $\rho_c$ through controlling the relative distribution of filler network.[5] In this case, the conductivity of CPCs basically depends on the morphology of polymer blends and the distribution state of fillers, which is governed by the process method and the filler affinity to a certain polymer or the interface. When the filler-rich phase percolates in the blends and the fillers form a network within the percolated blend phase, the conductivity of CPCs can be greatly enhanced. The phenomenon is called double percolation. Recently, carbon black (CB), carbon nanotubes (CNTs), graphene have been introduced into a number of immiscible polymer blends, such as poly(lactic acid)/poly($\varepsilon$-caprolactone) (PLA/PCL),[6] polyethylene/polycarbonate (PE/PC),[7] acrylonitrile-butadiene-styrene/polyamide-6 (ABS/PA6),[8] polystyrene/poly(methyl methacrylate) (PS/PMMA),[9] to achieve the optimal balance between high electrical performance and low fillers loading. Thermal-induced phase separation of partially miscible polymer blend matrix could be used as an efficient tool to control the dispersion state of conductive fillers and further enhance their conductive performance as well.[10] Furthermore, the distribution of fillers is affected by the morphology of blend matrix, but in turn may become a factor on their morphology not to be ignored. Many studies have reported that the introduction of nanoparticles may change the compatibility of immiscible polymer blends and stabilize their morphology, especially when the fillers locate at the interface of different phases.[11-14] Hence, for a better comprehension of the relationship between the morphology and conductivity of double percolated nanocomposites induced by phase separation, it is of great academic and industrial significance to investigate the phase behavior of ternary nanocomposites with a partially miscibe polymer blend matrix.

The aspect ratio of conductive fillers is another major factor that contributes to the $\rho_c$ of CPCs. CNTs are considered as preferable conductive nanofillers due to their large aspect ratio and high

electrical conductivity, which may form an interconnected network at a relatively low $\rho_c$. Furthermore, the abundance of π-electron clouds and the large specific surface area of CNTs facilitate the interactions with the polymer matrix. Based on the statement abovementioned, multi-walled carbon nanotubes (MWNTs) are chosen as the conductive fillers to be incorporated into a lower critical solution temperature (LCST) type polymer blend to explore the evolution relationship between the morphology and conductivity of ternary nanocomposites. Notably, the effect of CNTs which are rather flexible coiled rod-like particles needs more understanding on the phase separation behavior of blend matrix. Then, the effective control for the morphology of blend matrix and selective distribution of CNTs can be achieved to improve the electrical conductivity of CPC materials.

Dynamic rheological measurement is often used to investigate the phase separation behavior and the aggregation process of fillers because it is sensitive to the morphology evolution as well as the dispersion variation of nanoparticles.[15, 16] However, in the ternary filled nanocomposites with a partially miscibe polymer blend matrix, the contributions from the phase separation of blend matrix and the aggregation of nano-fillers to dynamic modulus are present at the same time and hard to distinguish only by rheological measurement. Simultaneous measurement of rheological and conductive properties could provide the real-time variation of viscoelastic and conductive behaviors induced by the variation of microscopic condensed structure in the different external field (thermal field, shear field).[17-20] In this paper, we adopt this method to record the synchronous evolution of volume resistivity ($\rho$) and dynamic storage modulus ($G'$) for MWNTs filled partially miscible blends of poly(methyl methacrylate)/poly(styrene-*co*-acrylonitrile) (PMMA/SAN) subjected to annealing above the phase separation temperature, and then pursue the aggregation of MWNTs and the morphology evolution of blend matrix. We attempt to clarify the effect of MWNTs on the phase separation behaviors of PMMA/SAN blend matrix and distinguish the respective contributions of MWNTs agglomeration and matrix phase separation on $G'$. The variations in $\rho$ and $G'$ as a function of filler content and temperature are also studied for systematically understanding the interaction between the abovementioned two behaviors of the nanocomposites during annealing.

## 2. Experimental

### 2.1. Materials

Poly (methyl methacrylate) (PMMA) (IF850, $M_w = 7.5\times10^4$, $M_w/M_n = 1.5$) was purchased from LG Chemical, Ltd., Korea. Poly (styrene-*co*-acrylonitrile) (SAN) (PN-127H, AN = 32 wt%, $M_w = 1.5\times10^5$, $M_w/M_n = 1.7$) was from Chimei Corporation, Taiwan. Multi-walled carbon nanotubes (MWNTs) (NC7000, average diameter of 9.5 nm, average length of 1.5 μm) were obtained from Nanocyl, Belgium. Analytical grade of tetrahydrofuran (THF) was obtained from commercial source and used as received.

### 2.2. Sample preparation

PMMA and SAN were dried for 6 h at 80 °C in an oven and MWNTs were also dried for 24 h in a vacuum oven before use to remove any moisture. MWNTs were dispersed in THF and the suspension was sonicated for 1 h with a power of 385W to break up the MWNT bundles. PMMA and SAN at different volume ratios were dissolved in the MWNT supensions at a weight fraction of 10 wt% to form the mixture solutions by stirring for 12 h at room temperature. The mixture was sonicated for another 1 h to achieve the uniform dispersion of MWNTs in PMMA/SAN blend solution. Subsequently the solutions were cast onto the surface of horizontal glass plates at 30 °C in an oven. After the solvent evaporated in an ambient environment of 30 °C for 1 day, the samples were further dried with steps at 90, 110 and 130 °C, respectively in a vacuum oven for at least 3 days to remove the residual solvent. These films with the thickness of about 100 μm were folded up and compression molded into the discs with the dimensions of 25 mm in diameter and 1.2 mm in thickness at 10 MPa and 130 °C for rheological measurements. PMMA/MWNTs and SAN/MWNTs binary nanocomposites were also prepared according to the similar procedures for the simultaneous measurement of rheological and conductive behaviors.

The samples for phase contrast microscopy (PCM) observation were prepared in the same way as above with an adjusted mixture solution weight fraction of 5 wt% and the solutions were dropped on the cover slips to form uniform films. The drying procedures of the films are in accord with the way above. The central thickness of the sample film was measured about 20μm. In the context below, we denote PMMA/SAN blends by A/B and PMMA/SAN/MWNTs nanocomposites by A/B/*x*, where A and B are the volume fraction of PMMA and SAN in the blends, respectively, and *x* is the volume content of MWNTs in the total polymer blends.

### 2.3 Characterization

The dispersion of MWNTs and morphological evolution of nanocomposites were observed by a transmission electron microscope (TEM, JEM 1200EX, Japan). The rheological test samples subjected to different isothermal annealing were quenched to maintain their morphology. TEM specimens were made by ultramicrotoming with a diamond knife at room temperature.

The morphological evolution of PMMA/SAN blends and PMMA/SAN/MWNTs nanocomposites was detected by phase contrast microscopy (PCM, B1-PH, Motic, China) in combination with a digital camera (Nikon-4500, Nikon, Japan). The samples were isothermally annealed at 190 $^{o}$C. All the morphological images were recorded in real time online.

Dynamic rheological tests were performed on an advanced rheometric expanded system (ARES, TA Instruments Corporation, USA) with parallel plate geometry of 25 mm in diameter. Isothermal frequency sweeps ranging from 100 rad·s$^{-1}$ to 0.01 rad·s$^{-1}$ were performed at various temperatures ranging from 150 to 180 $^{o}$C. The strain in the tests was set to 1% ensuring that all the

measurements were in the linear viscoelastic region.

The setup for simultaneous measurement of rheological and electrical behaviors was mentioned elsewhere[21, 22] and wasn't described in details here. The samples were annealed at 60 °C for 24 h to relieve the internal stress before simultaneous measurements. Rheological measurements were also performed on an advanced rheometric expanded system (ARES, TA Instruments Corporation, USA) with parallel plate geometry of 25 mm in diameter and volume resistance was simultaneously measured by a digital picoammeter (Keithley 6487, Keithley Instruments Inc., USA). Dynamic time sweep tests were conducted with a frequency ($\omega$) of 0.3 rad·s$^{-1}$ at 1% strain and various temperatures ranging from 170 to 200 $^{o}$C by a step of 10 $^{o}$C and the applied direct voltage was less than 10V. Previous experiments with various strain amplitudes confirmed that the influence of 1% strain amplitude on resistance was negligible.[23]

## 3. Results and discussion

### 3.1 Dispersion of MWNTs and morphology evolution of nanocomposites

TEM micrographs of 0.2 vol% MWNTs filled PMMA, SAN and PMMA/SAN (57/43) nanocomposites without annealing are shown in Figure 1. MWNTs are almost well dispersed in the three nanocomposites and PMMA/SAN (57/43) matrix is homogenous, indicating that the incorporation of MWNTs hardly destroys the homogeneity of blend matrix. With more refined resolution, it can be found that MWNTs show pretty good and uniform dispersion in SAN and PMMA/SAN two homogeneous matrices (Figure 1(a) and 1(c)) and most of them even exist in the form of single tube. However, MWNTs in PMMA matrix are in a relative worse dispersion state with some obvious agglomerates, indicating that PMMA is relatively difficult to wet the MWNTs. It may be addressed to the bulky methyl acrylate side groups in PMMA, which may hinder infiltration and interactions of the polymer with the initial agglomerates.[24] Such different dispersion states of MWNTs in these three matrices may indicate that MWNTs have more affinity for SAN than for PMMA.

In order to explore the distribution variation of MWNTs during phase separation, the blend morphology and the corresponding dispersion state of MWNTs for PMMA/SAN/MWNTs (57/43/0.4) nanocomposites subjected to annealing at 180 $^{o}$C for different time were also observed by TEM, as shown in Figure 2. The bright region refers to the PMMA-rich phase and the dark region refers to the SAN-rich phase in the bright-field TEM micrographs. The co-continuous morphology can be observed in the PMMA/SAN blend matrix after being annealed for 100s, 1000s and 4h, indicating the emergence of phase separation according to the spinodal decomposition (SD) mechanism. Furthermore, MWNTs are almost dispersed in the SAN-rich domain (dark region) at the early stage of SD phase separation for PMMA/SAN blend matrix (Figure 2a). With the evolution of phase separation, MWNTs are still located in the gradually coarsening SAN-rich phase with a relatively aggregated state at the medium and late stages of SD (Figure 2(b) and 2(c)). Lee also found that MWNTs are mainly located at SAN domain regardless of the SAN compositions and the processing methods in PMMA/SAN blend.[25] Generally, from the

perspective of structure similarity, it is considered that $\pi$-$\pi$ stacking caused by the interaction between the phenyl-ring structure of SAN and the honeycomb of MWNTs is likely to increase the thermodynamic affinity,[25] resulting in the selective location of MWNTs in the SAN-rich phase. On the other hand, in an immiscible or partially miscible blend, the minimization of the interfacial energy is the thermodynamic driving force for the filler to localize in a specific phase or at the interface.[26] A quantitative estimation of wetting coefficient may give the idea about the selective localization of MWNTs in the blend matrix driven by the thermodynamic forces, providing the surface free energy of the components. It is well-known that according to the Young's equation, the location of filler in a polymer blend matrix can be also predicted by evaluating the wetting coefficient $\omega_a$.[27]

$$\omega_a = \frac{\gamma_{\text{filler-A}} - \gamma_{\text{filler-B}}}{\gamma_{\text{A-B}}} \quad (1)$$

where $\gamma_{i\text{-}j}$ is the interfacial tension between different components. The fillers are predicted to locate in the A-rich phase when $\omega_a < -1$, in the B-rich phase when $\omega_a > 1$ and at the inter-phase in the interval of $\omega_a$ value between -1 and 1. The harmonic mean equation is commonly used to calculate the interfacial tension between component pairs:

$$\gamma_{12} = \gamma_1 + \gamma_2 - 4\left[\frac{\gamma_1^d \gamma_2^d}{\gamma_1^d + \gamma_2^d} + \frac{\gamma_1^p \gamma_2^p}{\gamma_1^p + \gamma_2^p}\right] \quad (2)$$

Here, $\gamma_i$ is the surface tension of component $i$, $\gamma_i^d$ and $\gamma_i^d$ are the dispersive part and polar part of the surface tension of component $i$, respectivley. In this work, the surface tensions of PMMA, SAN and MWNTs with the same grade are extrapolated to the investigated temperatures using the temperature coefficients ($-d\gamma/dT$) extracted from the literatures.[28, 29] The interfacial tensions between component pairs and the wetting coefficients are calculated by using Eqs. (1) and (2) and summarized in Table 1. It is apparent that all the $\omega_a$ values are estimated to be higher than 1 in the investigated temperature region. Hence, the localization of MWNTs is energetically favored toward the SAN-rich phase. Such preferential location of one-dimensional MWNTs in the SAN-rich phase is very similar with that of another two-dimensional fuller carbon group nanofiller, graphene,[30] attributed to their similar chemical structures.

The selective localization of MWNTs in SAN-rich phase may enhance the effective volume of conductive fillers. Besides, the morphology evolution of blend matrix should be investigated to determine whether the double percolation can appear in the nanocomposites. Figure 3 shows the PCM photographs of PMMA/SAN (57/43) blends and PMMA/SAN/MWNTs (57/43/0.2) nanocomposites isothermally annealed at 190 $^{o}$C for different time. The unfilled and filled systems both exhibit a typical co-continuous structure at the early stage of SD phase separation and the domain sizes of the filled systems are remarkably smaller than those of the unfilled systems during the whole SD phase separation, indicating that the introduction of MWNTs may retard the

concentration fluctuation at the early stage and suppress the domain coarsening at the late stage. Furthermore, it can be found from Figure 3(b) and 3(d), the morphological pattern of unfilled system transforms from co-continuous to droplet structure due to the influence of interfacial tension between two polymer components,[31] as it is generally recognized that the co-continuous morphology is not a stable steady-state structure.[32] However, the co-continuous structure could exist in the filled system for a rather long time. Namely, the introduction of MWNTs stabilizes the co-continuous morphology and inhibits the transformation from percolation to droplet. The stabilizing effect of MWNTs on the phase morphology of blend matrix can be also found in other filled systems.[13, 33-35] The stable existing of such co-continuous structure may ensure the occurrence of double percolation.

### 3.2 Determination of the rheological phase diagram

Prior to the investigation on the effect of morphological evolution on the conductive property of ternary nanocomposites, their phase diagrams should be firstly obtained to distinguish the unstable regime (bicontinuous spinodal decomposition) and metastable regime (nucleation–growth-type (NG) phase separation). Hence, the matrix composition and annealing condition can be determined to ensure the continuous structure of MWNTs-rich domain. It is well known that for partially miscible polymer blends, their storage modulus ($G'$) shows different performances in the homogeneous region and phase-separated region or pre-transition region, especially at low frequencies ($\omega$s). Based on the sensitive response of viscoelastic change in polymer blends, rheology is regarded as an efficient tool to determine the phase separation temperature with a variety of protocols, regardless of the sample transparency.[36, 37] It is reported that for the systems with small difference in their glass transition temperatures, investigating the temperature dependence of viscoelastic behaviors though dynamic frequency sweeps may be more appropriate for the determination of phase separation temperature than that through dynamic temperature ramp tests because the enhancement of $G'$ due to the interface and concentration fluctuation is relatively small and easy to be covered by the decrease of $G'$ with the increasing temperature.[38] In general, the failure of time-temperature superposition (TTS) principle and the tail in the Cole-Cole curve can be used to determine the binodal temperature ($T_b$). It is suggested that the tail in the Cole-Cole curve is more sensitive to the phase separation behavior than the failure of TTS principle.[37] Such method is also applicable for nanoparticle filled blends in which the fillers do not affect the temperature dependence of moduli for blend matrix. In our work, the concentration (0.2 vol%) of MWNTs chosen here is too low to form the effective agglomeration at the early stage of phase separation which was determined by simultaneous measurement of rheological and electrical behaviors (discussed later in the text). Hence, the effect of 0.2 vol% MWNTs aggregation on the modulus of the nanocomposites at the early stage of phase separation can be neglected and the

contribution of morphology evolution to their modulus for such nanocomposite can be used to obtain their phase separation temperature. Here, the Cole-Cole curves of PMMA/SAN blends and PMMA/SAN/MWNTs nanocomposites are used to determine their $T_b$s. Figure 4 shows the Cole-Cole curves at different temperatures for PMMA/SAN (57/43) blends and PMMA/SAN/MWNTs (57/43/0.2) nanocomposites. The Cole-Cole curve can be divided into two parts by different relaxation mechanisms. In high $\omega$s region, the curve principally reflects the viscoelastic relaxation behavior of polymers, while the relaxation behavior in low $\omega$s may originate from the deformation of domain or particles. It is found that the Cole-Cole curves for the unfilled and filled systems are arc-shaped at low temperatures, indicating that the systems are homogeneous. When the temperature elevates, a tail emerges in low $\omega$ region, which indicates the appearance of another relaxation behavior.[32] As for the partially miscible systems, such phenomenon also refers in particular to the occurrence of phase separation. The more accurate determination of $T_b$ can be reached by reducing the temperature interval of frequency sweep. It is found that the tails appear near 165 $^oC$ for PMMA/SAN (57/43) blends and 167 $^oC$ for PMMA/SAN/MWNTs (57/43//0.2) nanocomposites. Hence, their $T_b$s could be deduced as 165 $^oC$ and 167 $^oC$, respectively.

Besides, dynamic isothermal frequency sweep measurements are also taken to determine another phase separation temperature, spinodal temperature ($T_s$) and such $T_s$s are independent on the heating rate. It is known that $T_s$ is usually obtained by dynamic temperature sweep tests based on the theoretical approach of Fredrickson and Larson.[39] However, $T_s$s obtained by this method are obviously dependent on the heating rate and inconsistent with our abovementioned $T_b$s are obtained from the isothermal measurements. At the early stage of SD phase separation, the system tends to form co-continuous structure, which is similar to the gel network structure. Hence, it is adoptable to apply the criterion for the critical gelation behavior in the blend with the co-continuous structure formed by SD mechanism.[11, 37, 40] The criterion suggests that the critical gel point is the temperature at which the tan $\delta$ vs. $\omega$ curve exhibits a zero-slope at low $\omega$s.[41, 42] Figure 5 shows the temperature dependence of tan $\delta$ at a series of frequencies for PMMA/SAN (57/43) blends and PMMA/SAN/MWNTs (57/43/0.2) nanocomposites. At the investigated four $\omega$s, their tan$\delta$ values all converge in a small temperature region, implying that tan$\delta$ becomes independent of frequency at a certain temperature. Hence, considering the experimental errors, the arithmetic mean of the intersections is used as $T_s$.

Based on the obtained $T_b$ and $T_s$, the apparent phase diagram of PMMA/SAN blends and PMMA/SAN/MWNTs nanocomposites is obtained, as shows in Figure 6. The effect of 0.2 vol% MWNTs on the phase separation temperatures remarkably depends on the compositions of blend matrix. When SAN is the minority of blend matrix (PMMA/SAN 57/43), the presence of 0.2 vol% MWNTs causes the increase of $T_b$ and $T_s$ for the nanocomposites; while when SAN is the majority, their $T_b$ and $T_s$ both decrease and their decline increases with the increasing SAN content. The

composition dependence of variation trend in $T_b$ and $T_s$ would be mainly attributed to the composition difference between the surface layer of MWNTs and blend matrix induced by the selective absorption of SAN on MWNTs. Here, it should be noted that in our previous research, PMMA/SAN 70/30 (w/w), namely PMMA/SAN 67/33 (v/v), is found to be the critical composition for such blend.[43] Hence, it can be understood that for PMMA/SAN/MWNTs (57/43/0.2) nanocomposites, the obvious increase of SAN content on the surface layer of MWNTs should result in the increase of their phase separation temperature. However, for PMMA/SAN/MWNTs (47/53/0.2) and PMMA/SAN/MWNTs (37/63/0.2) nanocomposites, the composition difference between the surface layer of MWNTs and blend matrix gradually reduces with the increasing SAN content and MWNTs may act as a nucleating agent to induce the occurrence of phase separation, resulting in the decrease of their $T_b$ and $T_s$. The similar phenomenon is also reported by Huang[11] and Gao[37] in PMMA/SAN/$SiO_2$-OH system and by Vleminckx[44] in P$\alpha$SAN/PMMA/TRG system. Hence, the interaction between nanoparticles and polymer chains, the selective distribution and concentration of nanofillers have considerable impacts in thermodynamics of phase separation.

### 3.3 Evolution of frequency dependent dynamic moduli during phase separation

Dynamic time sweep test under a specified frequency is usually adopted to monitor the phase separation and the aggregation of nanoparticles. However, time sweep can only give limited information at just one frequency as compared to the frequency dependence of dynamic moduli. Generally, cyclic frequency sweep and dynamic multiwave sweep can be used to follow the evolution of frequency dependent dynamic moduli during phase separation.[45] In our work, isothermal cyclic frequency sweep from 100 rad/s to 0.01 rad/s is chosen to investigate the effect of MWNTs on the phase separation behavior of PMMA/SAN blend matrix. It takes nearly 1 h for each cycle and usually 9 cycles are measured at the investigated temperature (The moduli tend to be constant after 9 cycles). Figure 7 (a) and 7 (b) show the evolution of storage modulus ($G'$) as a function of frequency at different cycles of PMMA/SAN (57/43) blends and PMMA/SAN/MWNT (57/43/0.2) nanocomposites during annealing at 180 $^oC$. Here, we only present the frequency dependence of $G'$, because the variation of $G'$ is more remarkable than that of loss modulus ($G''$) during phase separation.[36, 46] As it is clearly shown, the unfilled and filled system share the similarity that their $G'$ exhibits a distinct increment at high $\omega$s in the first two cycles and the increment slows down in the following cycles, indicating that the systems gradually tend to equilibrium. The variation of $G'$ for the blend at high $\omega$s may be just ascribed to the thermally induced local composition fluctuations inside the domains (component's contribution),[45] while that for the nanocomposite may be attributed to the aggregation of MWNTs in the SAN-rich domain as well.[47] On the other hand, the variation trends of $G'$ for the blend and nanocomposite at low $\omega$s with the increasing cycles are found to be just opposite. The platform of binary blend at

low $\omega$s is attributed to the emergence of co-continuous domain interface at the early stage of SD phase separation, while the shape relaxation of domain and the dissipative relaxation due to the space rearrangement of the aggregates could both behave as a second platform on the $G'$ curve of ternary composites. The decrease of $G'$ at low $\omega$s for the blend at 9 cycles is ascribed to the reduction of interfacial area with the increase of domain size (interfacial contribution),[36, 45, 48] while the obvious increase of $G'$ at low $\omega$s for the nanocomposite may be mainly caused by the aggregation of MWNTs in the SAN-rich domain, which may fully conceal the influence of growing domain on $G'$.[49-51]

To clearly clarify the effect of MWNTs on the frequency dependence of $G'$ variation, $G'$ at 0.01 rad·s$^{-1}$ and 0.25 rad·s$^{-1}$ as a function of annealing time for the unfilled and filled systems are extracted from Figure 7(a) and 7(b), respectively, as shown in Figure 7 (c). It can be seen from Figure 7(a) that there exists a crossover frequency (~0.045 rad·s$^{-1}$) where the moduli at different cycles are constant. The crossover frequency is thought as the boundary point to distinguish whether $G'$ is dominated by the interfacial contribution or the components' contribution.[45] Here, 0.01 and 0.25 rad·s$^{-1}$ are below and above the crossover frequency, respectively. It is obvious that the time evolution of $G'$ is strongly frequency dependent for the blend. $G'$ dominated by the interfacial contribution decreases slightly with the time at 0.01 rad·s$^{-1}$, while that dominated by the components' contribution increases with the time at 0.25 rad·s$^{-1}$. For ternary nanocomposites, their $G'$ values are much higher and the increments with the time are more obvious. Furthermore, the $G'$ values almost show the same increasing trend at two investigated frequencies, implying that the interfacial contribution and the components' contribution from the morphology evolution of blend matrix can be neglected and the contribution of MWNTs agglomeration may play the primary role. Hence, the time evolution of $G'$ for the nanocomposites hardly presents the remarkable frequency dependence.

### 3.4 Dynamic percolation of PMMA/SAN/MWNTs nanocomposites during isothermal annealing

Generally, the dispersion of nanoparticles in the molten polymer matrix is hardly in thermodynamic equilibrium state and they always tend to aggregate together for the reduction of excess interfacial energy.[21, 22, 52] The driving force for the aggregation of fillers might be the strong dispersive interaction between the filler and polymer matrix as well as the depletion interaction between the adjacent nanoparticles.[21, 22] In our study, simultaneous measurements of rheological and conductive properties were carried out to track the real time evolution of the dynamic modulus ($G'$) and the volume resistivity ($\rho$) for the unfilled and filled systems during isothermal annealing. As mentioned above, MWNTs are selectively localized in the SAN-rich phase and the minor SAN-rich domain should be maintained as continuous structure to ensure that small amount of MWNTs can form the continuous conductive pathway in CPC preparation. Here, the

composition of blend matrix was selected as PMMA/SAN 57/43 (near-critical composition) and the samples were isothermally treated well above $T_s$ (from Section 3.2). Figure 8 shows the time evolution of $\rho$ for neat PMMA, SAN, PMMA/SAN (57/43) blend and MWNTs filled nanocomposites at 180°C. During annealing, the $\rho$ value of PMMA shows about an order of magnitude reduction and those of PMMA/SAN blend and SAN almost remain stable, indicating that the presence of SAN may enhance the thermal stability of electrical property for the blends. The initial $\rho$ values of PMMA/SAN/MWNTs (57/43/0.2) and SAN/MWNTs (100/0.2) nanocomposites are in the same magnitude with their corresponding polymer matrices. With the extension of annealing time, the $\rho$ value drops sharply after a critical time defined as dynamic percolation time ($t_{pR}$), at which the first conductive pathway forms. Such sharp decline in $\rho$ is referred to dynamic conduction (DC) percolation.[52] There is no initial platform for PMMA/MWNTs (100/0.2) nanocomposite and its $\rho$ value reaches an equilibrium value after 300 s, indicating that a relatively perfect conductive network of MWNTs may form in the sample preparation. SAN/MWNT (100/0.2) nanocomposite possesses a much gradual reduction rate and a higher equilibrium $\rho$ value. The difference mainly results from a combination of the dispersion state of MWNTs, interfacial tension between the polymer and MWNTs as well as the interaction between adjacent MWNT particles. As we know from the Section 3.1, MWNTs are in a worse dispersion state in PMMA matrix with a lot of aggregates. Therefore, a much advanced percolation behavior happens in PMMA/MWNTs (100/0.2) nanocomposite. It can be found in Figure 1(b) and (c), the dispersion state of MWNTs in homogenous blend matrix is very similar to that in SAN. Compared with SAN/MWNTs (100/0.2) nanocomposite, the $\rho$ values of PMMA/SAN/MWNTs (57/43/0.2) ternary nanocomposite decrease more rapidly at a shorter $t_{pR}$ and finally reach a far lower equilibrium volume resistivity. The formation of double percolation in ternary nanocomposites, namely, the selective location for MWNTs in SAN-rich phase of a co-continuous polymer blend to form a percolated network in the selected phase, brings about an enhancement of effective loading and contributes to the reduction of final equilibrium $\rho$.

The filler content in SAN/MWNTs (100/0.4) nanocomposites is close to the effective content for PMMA/SAN/MWNTs (57/43/0.2) systems and the $t_{pR}$ of ternary system falls in between those of 0.2 and 0.4 vol% MWNTs filled SAN systems. Such phenomenon suggests that phase separation might emerge before $t_{pR}$, and most MWNTs migrate into the SAN-rich phase with the evolution of phase separation and then agglomerate to form the conductive network. The selective dispersion of MWNTs in the SAN-rich domain is just due to the better affinity between SAN and MWNTs, confirmed by the TEM characterization and the estimation of wetting coefficient. Furthermore, the exact sequence for phase separation of blend matrix and dynamic conduction percolation should be further confirmed by the TEM observation for the samples annealed above $T_s$ prior to $t_{pR}$. In brief, apart from the effect of thermal treatment on the aggregation of conductive fillers, the phase separation and morphology evolution of blend matrix may also play a role in the

conductive behavior of ternary nanocomposites.

The simultaneous evolution of rheological response for MWNTs filled SAN nanocomposites, PMMA/SAN (57/43) blends and PMMA/SAN/MWNTs (57/43/0.2) nanocomposites during annealing at 180 $^{o}$C and 0.3 rad·s$^{-1}$ is shown in Figure 8(c) to clarify the contributions of phase separation and filler agglomeration, respectively, to the evolution of modulus. Owing to the migration and aggregation of MWNTs in the SAN-rich phase during phase separation, the time evolution of $G'$ for SAN/MWNTs systems are just given and set as a comparison. The $G'$ values in the first 100s were removed due to the turbulence of heat transmission between the environment and the sample. For all the systems, $G'$ values gradually raises with the annealing time before they approach a steady value, which is defined as dynamic modulus (DM) percolation and $t_{pG}$ is the critical time above which $G'$ varies markedly.[17, 21] However, there are different origins resulting in the DM percolation for such four systems. For PMMA/SAN (57/43) blends, $G'$ increases after $t_{pG}$ at the frequency of 0.3 rad·s$^{-1}$ (above the crossover frequency) due to the thermally induced local composition fluctuations inside the domains (component's contribution), as mentioned in Section 3.2. SAN/MWNTs (100/0.2) nanocomposites show marked DM percolation behavior due to the agglomeration of MWNTs. The interaction between MWNTs and SAN restricts the aggregation of MWNTs in the SAN matrix, which leads to a gentle increment of $G'$. Compared with SAN/MWNT (100/0.2) nanocomposites, PMMA/SAN/MWNTs (57/43/0.2) nanocomposites reveal a more remarkable DM percolation behavior with a shorter $t_{pG}$, and a tremendous increase in $G'$. For ternary system, $G'$ starts to increase dramatically at about 500 s, which is close to the $t_{pG}$ of PMMA/SAN (57/43) polymer blends (<500 s), while $G'$ for SAN/MWNTs (100/0.2) nanocomposites increases remarkably after 700 s, suggesting that the presence of MWNTs may slightly retard the SD phase separation of blend matrix and the increment of $G'$ ($t$ < 700 s) may be ascribed to the components' contribution induced by the SD phase separation of blend matrix.[45] The following increment of $G'$ for PMMA/SAN/MWNTs (57/43/0.2) nanocomposites is regarded as the superimposition of phase coalescence for blend matrix and MWNTs agglomeration.[19, 20] Here, the modulus increment due to MWNTs aggregation may be mainly attributed to the reduction in the macromolecular mobility of blend matrix induced by the direct bridging of single chains adsorbed on different MWNTs aggregates, the entanglement between chains adsorbed on separate aggregates and the entanglement of non-adsorbed bulk chains.[53, 54] Moreover, $G'$ of PMMA/SAN/MWNTs (57/43/0.2) system at the late stage of annealing is higher than that of SAN/MWNTs (100/0.2) system and close to that of SAN/MWNTs (100/0.4) system. Here, it should be noted that the selective distribution of MWNTs in the SAN-rich domain results in the condensed agglomeration network of MWNTs with the effective volume content of 0.465. In order to specifically clarify the respective contribution of phase separation and MWNTs aggregation, $G'$ evolution curves for the unfilled and filled systems are normalized in the insert plot of Figure 8 (c). It is clearly observed that the increase amplitude of $G'$ for the blend is the smallest and those for

MWNTs filled SAN nanocomposites increase with the increasing loadings of MWNTs. However, the increase amplitude for ternary nanocomposites, especially at the medium and late stage of annealing is almost the superimposition of those for the blend and SAN/MWNTs (100/0.4), rather than SAN/MWNTs (100/0.2) nanocomposite. Furthermore, the contribution of modulus increment mainly comes from the agglomeration of MWNTs and the contribution from phase separation of blend matrix just presents fairly at the initial stage of annealing.

The formation of conductive network in a filled system also depends on the annealing temperature.[55] Figure 9 exhibits the synchronous evolution of $\rho$ and $G'$ for PMMA/SAN/MWNTs (57/43/0.2) nanocomposites at various annealing temperatures. When the annealing temperature elevates, their $t_{pR}$ and $t_{pG}$ reduce markedly and their $\rho$ and $G'$ values tend to approach the equilibrium state more quickly, reflecting that high temperature can accelerate the DC and DM percolation behaviors. Nevertheless, the variation of $t_{pG}$ with temperature is less obvious than that of $t_{pR}$, indicating a limited acceleration effect of annealing temperature on the DM percolation.

Due to the weak contribution of phase separation for blend matrix to dynamic modulus, it is difficult to determine the order for the phase separation of blend matrix and the aggregation of MWNTs into conductive network only by simultaneous measurement of rheological and electrical behaviors. TEM micrographs of the samples annealed prior to $t_{pR}$ should be provided to further confirm the sequence of two abovementioned behaviors. Figure 10 (a), (b) and (c) show the TEM images of PMMA/SAN/MWNTs (57/43/0.2) nanocomposites after being annealed for 500 s at 170 $^{o}$C 300s at 180 $^{o}$C and 200 s at 190 $^{o}$C, respectively. It can be found that the blend matrix shows co-continuous morphology and most MWNTs migrate into the SAN-rich phase before $t_{pR}$ at all the investigated annealing temperatures, implying that the phase separation of matrix occurs prior to the DC percolation. Krasovitski et al. proposed that for the particles with high aspect ratio, even very small differences in wetting behavior are sufficient for complete penetration into the better wetting liquid.[56] Hence, it is easy for MWNTs to migrate into the SAN-rich phase even being annealed for a rather short time period. The aggregation of MWNTs in the SAN-rich phase plays a predominant role in the conductivity evolution. It may account for the self-similarity of $\rho$-$t$ curves of ternary nanocomposites at different temperatures, which is commonly found in the nanocomposites with unitary polymer matrix. Furthermore, it can be found from Figure 8(b) that the absolute value for the slope of $\rho$ reduction of ternary system is larger than those for 0.2 and 0.4 vol% MWNTs filled SAN systems, indicating that the restriction of MWNTs in the fine SAN domain at the early stage of SD phase separation may lead to an increment of the contact randomness and opportunity between adjacent MWNTs. Hence, the real content of MWNTs and $t_{pR}$ for PMMA/SAN/MWNTs (57/43/0.2) system are both smaller than those for SAN/MWNTs (100/0.4) system, but the further agglomeration of ternary system is much faster and more effective than that of SAN/MWNTs (100/0.4) system, resulting in the lower equilibrium $\rho$ value.

Filler content is also thought to play an important role on $t_{pR}$, $\rho$ and dynamic modulus of the

nanocomposites. Figure 11 shows the DC and DM percolation behaviors of PMMA/SAN/MWNTs nanocomposites with various filler volume fractions at 180 °C. The thermal DC percolation is related to the rearrangement of MWNT aggregates to form continuous conductive pathways after $t_{pR}$ and $t_{pR}$ decreases sharply with increasing $\phi$. Meanwhile, the DM percolation behavior becomes more intensive and $t_{pG}$ reduces with increasing $\phi$. It is known that the incorporation of nanofiller may stabilize the phase structure of blend matrix through the retardation of macromolecular diffusion and the hinder effect may enhance with the increase of filler loadings.[30, 43, 57, 58] Hence, the effect of MWNTs content on the contribution of modulus increment arising from the phase separation of blend matrix can be neglected. At a given time, especially in the medium and late stages of annealing, the increment of $G'$ with increasing $\phi$ may be mainly ascribed to the hydrostatic reinforcement effect. The decline of $t_{pR}$ and $t_{pG}$ indicates that the increase of MWNTs content may accelerate the dynamic percolation.[17]

The time evolution of $\rho$ for PMMA/SAN/MWNTs (57/43/x) nanocomposites with the filler loadings of 0.1 and 0.4vol% at different annealing temperatures were also investigated (Figure 12 (a) and 12 (b)) to explore the temperature dependence of their DC percolation behavior. The $t_{pR}$ values for PMMA/SAN/MWNTs (57/43/0.1) and PMMA/SAN/MWNTs (57/43/0.4) nanocomposites can be easily obtained from Figure 12 (a) and 12 (b). Figure 12 (c) shows the critical time $t_{pR}$ as a function of reciprocal temperature ($1/T$) for PMMA/SAN/MWNTs (57/43/x) nanocomposites. It is obvious that the ln $t_{pR}$ vs. $1/T$ plots for three nanocomposites show good linearity and are parallel to each other. The activation energy of the DC percolation, $\Delta E_R$ is determined from the slope of $t_{pR}$ against $1/T$ and shown in Figure 12 (c). $\Delta E_R$ is nearly independent on $\phi$ at $\phi$ = 0.1-0.4 vol% and the value of $\Delta E_R$s with 13% maximal error are close with each other. It is reported that the aggregation of CB in unitary polymer melts has a close relationship with polymer dynamics.[59, 60] Although the polymer matrix is a binary blend in this work, the phase separation of PMMA/SAN blend matrix occurs prior to the DC percolation and then MWNTs migrate rapidly and aggregate in the SAN-rich phase. To compare the activation energies of DC percolation for the nanocomposites and viscous flow of SAN, we measured the dynamic modulus for SAN as a function of $\omega$ at the temperature range of 150-200 °C. Figure 13 (a) shows the master curves of $G'$ and $G''$ for SAN at the reference temperature of 170 °C. Figure 13 (b) shows the horizontal shift factor, $\alpha_T$, used for constructing the master curves, as a function of $1/T$, indicating that the temperature dependence of $\alpha_T$ for SAN fits the Arrhenius equation with the activation energy of flow ($\Delta E_{\alpha T}$) of 181.9 ± 6.3 kJ·mol$^{-1}$. It is observed that the $\Delta E_R$ for the DC percolation is very close to $\Delta E_{\alpha T}$ for the viscous flow of SAN, indicating that the DC percolation is related to the mobility and the structure of SAN matrix. Such phenomenon is similar with some earlier results reported by other researchers in the composites with unitary polymer matrix.[59, 60] Wu et al. investigated the DC percolation of CB-filled polymers and revealed that $\Delta E_R$ is closely related to activation energy of zero-shear rate viscosity ($\eta_0$) of the matrix.[59] Otherwise, Zhang et al.

revealed that $\Delta E_R$ approaches the activation energy of $\eta_0$ of filled polymer composites.[60] Here, the contact process between two MWNTs is equivalent to the excluding process of polymer molecules between two particles essentially.[59] Hence, the mobility of MWNTs in the phase-separated blend matrix could reflect the mobility of polymer layer, SAN, surrounding MWNTs, while it is hardly related to the mobility of PMMA.

Obviously, the morphology evolution of PMMA/SAN blend matrix might facilitate the redistribution and effective agglomeration of MWNTs in the SAN-rich phase during SD phase separation process to increase the effective volume content of MWNTs in ternary nanocomposites. Furthermore, the MWNTs in the minor SAN phase can retard its morphology transition from percolation to droplet structure and maintain the continuous dispersion in the phase separated blend matrix. The DC and DM percolations for PMMA/SAN/MWNTs nanocomposites result from different mechanisms. The DC percolation just reflects the formation of MWNTs conductive network in PMMA/SAN blend, while the DM percolation reflects the total contributions from the morphology evolution of blend matrix, the MWNTs migration and agglomeration in the SAN-rich phase. Although both the DC percolation and the DM percolation are involved in the movement of MWNTs aggregates, the temperature dependence of $t_{pG}$ for such system is more complicated and will be further explored in our next work.

## 4. Conclusions

The morphology evolution, conductive and viscoelastic behaviors of PMMA/SAN/MWNTs nanocomposites have been monitored during annealing by melt rheology, simultaneous measurements of rheological and conductive properties and microscopic techniques. With the occurrence of phase separation for PMMA/SAN blend matrix upon annealing, the MWNTs well-dispersed in homogeneous blend matrix rapidly migrate into the SAN-rich domains and then gradually form the MWNTs conductive network, owing to the affinity of MWNTs to SAN. The effect of MWNTs on the phase separation temperatures of PMMA/SAN blend depends on the composition of blend matrix. Namely, when SAN is the minority of blend matrix, the presence of 0.2 vol% MWNTs causes the increase of $T_b$ and $T_s$ for the nanocomposites; while when SAN is the majority, their $T_b$ and $T_s$ both decrease and their decline increases with the increasing SAN content. Such composition dependence may be the result of the composition difference between surface layer of MWNTs and polymer matrix induced by the selective absorption of SAN on the surface of MWNTs. Furthermore, the introduction of MWNTs significantly depresses the morphology evolution of blend matrix and effectively maintains the initial co-continuous phase structure for ensuring the formation of double percolation.

Synchronous evolution of $G'$ and $\rho$ for PMMA/SAN/MWNTs nanocomposites upon isothermal annealing well above $T_s$ shows the more remarkable DM and DC percolation behaviors. The origin of their DM percolation is more complicated than that of DC percolation, which is a

combined effect of morphology evolution of polymer matrix and the aggregation of MWNTs. Further investigation may distinguish the respective contribution of morphology evolution of matrix and MWNTs agglomeration to their dynamic modulus, in which phase separation predominates in the initial stage of annealing and the flocculation of MWNTs accounts dominantly in the following stage. The activation energies of $t_{pR}$ for ternary nanocomposites are found close to that of viscous flow for SAN, suggesting that the mobility of MWNTs in the phase-separated blend matrix is indeed controlled by the mobility of SAN surrounding MWNTs. Hence, the redistribution of MWNTs in the matrix induced by SD phase separation of PMMA/SAN blend results in the formation of double percolation and the dramatic insulation-to-conduction transition at the lower percolation threshold. Thermal-induced phase separation of partially miscible blend matrix may provide a simple and effective way to fabricate CPCs with the desired electrical performance.

## Acknowledgements

This work was financially supported by the National Natural Science Foundation of China (Nos. 51273173 and 51003093) and the National Natural Science Foundation of Zhejiang Province (No. LY16E030001).

## Notes and references

1. M. H. Al-Saleh and U. Sundararaj, *Carbon*, 2009, **47**, 2-22.
2. H. Deng, L. Lin, M. Ji, S. Zhang, M. Yang and Q. Fu, *Prog. Polym. Sci.*, 2014, **39**, 627-655.
3. S. Razdan, P. K. Patra, S. Kar, L. Ci, R. Vajtai, A. Kukovecz, Z. Konya, I. Kiricsi and P. M. Ajayan, *Chem. Mater.*, 2009, **21**, 3062-3071.
4. H. Deng, T. Skipa, E. Bilotti, R. Zhang, D. Lellinger, L. Mezzo, Q. Fu, I. Alig and T. Peijs, *Adv. Func. Mater.*, 2010, **20**, 1424-1432.
5. C. Gao, S. Zhang, F. Wang, B. Wen, C. Han, Y. Ding and M. Yang, *ACS Appl. Mater. Inter.*, 2014, **6**, 12252-12260.
6. J. R. Huang, C. Mao, Y. T. Zhu, W. Jiang and X. D. Yang, *Carbon*, 2014, **73**, 267-274.
7. P. Pötschke, A. R. Bhattacharyya and A. Janke, *Polymer*, 2003, **44**, 8061-8069.
8. G. Wu, B. Li and J. Jiang, *Polymer*, 2010, **51**, 2077-2083.
9. C. Mao, Y. T. Zhu and W. Jiang, *ACS Appl. Mater. Inter.*, 2012, **4**, 5281-5286.
10. S. Bose, C. Ozdilek, J. Leys, J. W. Seo, M. Wubbenhorst, J. Vermant and P. Moldenaers, *ACS Appl. Mater. Inter.*, 2010, **2**, 800-807.
11. C. W. Huang, J. P. Gao, W. Yu and C. X. Zhou, *Macromolecules*, 2012, **45**, 8420-8429.
12. G. P. Kar, P. Xavier and S. Bose, *Phys. Chem. Chem. Phys.*, 2014, **16**, 17811-17821.
13. W. Li, R. M. A. l'Abee and J. G. P. Goossens, *Macromol. Chem. Phys.*, 2013, **214**, 2705-2715.
14. P. P. Vijayan, D. Puglia, J. M. Kenny and S. Thomas, *Soft Matter*, 2013, **9**(10), 2899-2911.

15. M. Zuo and Q. Zheng, *Sci. China Ser. B: Chem*, 2008, **51**, 1-12.
16. F. S. Zou, X. Dong, W. Liu, D. J. Wang and C. C. Han, *Chin. J. Polym. Sci.*, 2014, **32**, 718-730.
17. Q. Cao, Y. H. Song, Y. Q. Tan and Q. Zheng, *Carbon*, 2010, **48**, 4268-4275.
18. Q. Cao, Y. H. Song, Z. H. Liu and Q. Zheng, *J. Mater. Sci.*, 2009, **44**, 4241-4245.
19. Y. H. Song, C. F. Xu and Q. Zheng, *Soft Matter*, 2014, **10**, 2685-2692.
20. Y. Tan, Y. Song, Q. Cao and Q. Zheng, *Polym. Int.*, 2011, **60**, 823-832.
21. Q. Cao, Y. Song, Y. Tan and Q. Zheng, *Polymer*, 2009, **50**, 6350-6356.
22. Y. Song, Q. Cao and Q. Zheng, *Colloid Polym. Sci.*, 2012, **290**, 1837-1842.
23. I. Alig, T. Skipa, D. Lellinger and P. Pöetschke, *Polymer*, 2008, **49**, 3524-3532.
24. I. Alig, P. Pötschke, D. Lellinger, T. Skipa, S. Pegel, G. R. Kasaliwal and Villmow T. *Polymer*, 2012, **53**, 4-28.
25. M. Lee, H. Jeon, B. H. Min and J. H. Kim, *J. Appl. Polym. Sci.*, 2011, **121**, 743-749.
26. M. Sumita, K. Sakata, S. Asai, K. Miyasaka and H. Nakagawa, *Polym. Bull.*, 1991, **25**, 265-271.
27. S. Wu, *J. Polym. Sci. Part C-Polym. Symp.*, 1971, **34,** 19-30.
28. M. A. Sawpan, Z. Funke, M. Weber, H.-W. Kammer and J. Kressler, *Macromol. Chem. Phys.*, 2009, **210**, 60-68.
29. K. W. Stöeckelhuber, A. Das, R. Jurk and G. Heinrich, *Polymer*, 2010, **51**, 1954-1963.
30. C. Y. Lin, M. Zuo, H.-h. Li, T. Liu and Q. Zheng, *Chin. J. Polym. Sci.*, 2015, **33**, 1162-1175.
31. H. S. Jeon, A. I. Nakatani, C. C. Han and R. H. Colby, *Macromolecules*, 2000, **33**, 9732-9739.
32. D. F. Wu, Y. S. Zhang, M. Zhang and W. D. Zhou, *Euro. Polym. J.*, 2008, **44**, 2171-2183.
33. P. Xavier and S. Bose, *J. Phys. Chem. B*, 2013, **117**, 8633-8646.
34. T. Sun, X. Dong, K. Du, K. Wang, Q. Fu and C. C. Han, *Polymer*, 2008, **49**, 588-598.
35. J. K. Yeganeh, F. Goharpey, E. Moghimi, G. Petekidis and R. Foudazi, *Soft Matter*, 2014, **10**, 9270-9280.
36. M. Zuo and Q. Zheng, *Macromol. Chem. Phys.*, 2006, **207**, 1927-1937.
37. J. Gao, C. Huang, N. Wang, W. Yu and C. Zhou, *Polymer*, 2012, **53**, 1772-1782.
38. R. M. Li, W. Yu and C. X. Zhou, *Chem. J. Chin.Univ.*, 2006, **1**, 166-169.
39. G. H. Fredrickson and R. G. Larson, *J. Chem. Phys.*, 1987, **86**, 1553-1560.
40. I. S. Polios, M. Soliman, C. Lee, S. P. Gido, K. Schmidt-Rohr and H. H. Winter, *Macromolecules*, 1997, **30**, 4470-4480.
41. A. Kelarakis, K. Yoon, R. H. Somani, X. M. Chen, B. S. Hsiao and B. Chu, *Polymer*, 2005, **46**, 11591-11599.
42. S. Huang, Z. Liu, C. Yin, Y. Gao, Y. Wang and M. Yang, *Polymer*, 2012, **53**, 4293-4299.
43. M. Du, Q. Wu, M. Zuo and Q. Zheng, *Euro. Polym. J.*, 2013, **49**, 2721-2729.
44. G. Vleminckx, S. Bose, J. Leys, J. Vermant, M. Wubbenhorst, A. A. Abdala, C. Macosko and P.

Moldenaers, *ACS Appl. Mater. Inter.*, 2011, **3**, 3172-3180.

45. Y. Xu, C. Huang, W. Yu and C. Zhou, *Polymer*, 2015, **67**, 101-110.
46. A. Ajji and L. Choplin, *Macromolecules*, 1991, **24**, 5221-5223.
47. G. Filippone and M. S. de Luna, *Macromolecules*, 2012, **45**, 8853-8860.
48. J. K. Yeganeh, F. Goharpey and R. Foudazi, *Macromolecules*, 2010, **43**, 8670-8685.
49. Y. Song and Q. Zheng, *J. Rheol.*, 2015, **59**, 155-191.
50. G. Filippone, G. Romeo and D. Acierno, *Langmuir*, 2010, **26**, 2714-2720.
51. T. Xia, Y. Huang, X. Jiang, Y. Lv, Q. Yang and G. Li, *Macromolecules*, 2013, **46**, 8323-8333.
52. G. Z. Wu, S. Asai, C. Zhang, T. Miura and M. Sumita, *J. Appl. Polym. Sci.*, 2000, **88**, 1480-1487.
53. S. Bar-Chaput and C. Carrot, *Rheol. Acta*, 2006, **45**, 339-347.
54. P. Cassagnau and F. Melis, *Polymer*, 2003, **44**, 6607-6615.
55. C. Zhang, P. Wang, C.A. Ma, G. Wu and M. Sumita, *Polymer*, 2006, **47**, 466-473.
56. B. Krasovitski and A. Marmur, *J. Adhes.*, 2005, **81**, 869-880.
57. D. Z. Pang, M. Zuo, J. S. Zhao and Q. Zheng, *Chin. J. Polym. Sci.*, 2013, **31**, 1470-1483.
58. C. Y. Lin, T. Liu, M. Zuo, H. H. Li, Q. Chen and Q. Zheng, *Rsc Adv.*, 2015, **5**, 82259-82270.
59. G. Z. Wu, S. Asai and M. Sumita, *Macromolecules*, 2002, **35**, 1708-1713.
60. C. Zhang, L. Wang, J. Wang and C.A. Ma, *Carbon*, 2008, **46**, 2053-2058.

**Figure Captions**

**Figure 1.** TEM micrographs of (a) PMMA/MWNT (100/0.2), (b) SAN/MWNT (100/0.2) and (c) PMMA/SAN/MWNT (57/43/0.2) nanocomposites without annealing.

**Figure 2.** TEM micrographs of PMMA/SAN/MWNT (57/43/0.4) nanocomposites annealed at 180 $^{o}$C for (a) 100 s, (b) 1000 s and (c) 4 h.

**Figure 3.** Morphology evolution of (a) (b) (c) (d) PMMA/SAN (57/43) blend and (a´) (b´) (c´) (d´) PMMA/SAN/MWNT (57/43/0.2) nanocomposite under annealing at 190 $^{o}$C for different time.

**Figure 4.** Cole-Cole plots of (a) PMMA/SAN (57/43) blend and (b) PMMA/SAN/MWNT (57/43/0.2) nanocomposite at different temperatures.

**Figure 5.** Temperature dependence of tan $\delta$ under different frequencies (0.01~0.040 rad·s$^{-1}$) for (a) PMMA/SAN (57/43) blend and (b) PMMA/SAN/MWNT (57/43/0.2) nanocomposite.

**Figure 6.** Apparent phase diagram of PMMA/SAN blends and 0.2 vol% MWNT filled PMMA/SAN nanocomposites.

**Figure 7.** Dynamic storage modulus ($G'$) under cyclic frequency sweeps at 180 °C for (a) PMMA/SAN (57/43) blends and (b) PMMA/SAN/MWNT (57/43/0.2) nanocomposites; (c) $G'$ for the unfilled and filled systems as a function of time ($t$) at 180 °C at 0.25 rad·s$^{-1}$ and 0.01 rad·s$^{-1}$.

**Figure 8.** Time evolution of volume resistivity $\rho$ for (a) unfilled PMMA,SAN, PMMA/SAN (57/43) systems, (b) MWNT filled PMMA, SAN, PMMA/SAN (57/43) nanocomposites; (c) time evolution of dynamic storage modulus $G'$ at 180 °C. The insert plot shows the normalized dynamic modulus $G'/ G'_0$ at 180 °C.

**Figure 9.** Time evolution of (a) $\rho$ and (b) $G'$ for PMMA/SAN/MWNT (57/43/0.2) nanocomposites at different annealing temperatures.

**Figure 10.** TEM micrographs of PMMA/SAN/MWNT (57/43/0.2) nanocomposites annealed at (a) 170 $^{o}$C for 500 s, (b) 180 $^{o}$C for 300 s and (c) 190 $^{o}$C for 200 s.

**Figure 11.** Time evolution of (a) $\rho$ and (b) $G'$ for PMMA/SAN/MWNT (57/43/x) nanocomposites with different MWNT volume fractions $\phi$ at 180 °C.

**Figure 12.** Time evolution of $\rho$ for (a) PMMA/SAN/MWNT (57/43/0.1) and (b) PMMA/SAN/MWNT (57/43/0.4) nanocomposites at different annealing temperatures. (c) $\ln t_{pR}$ as a function of $1/T$ for MWNT filled PMMA/SAN (57/43) nanocomposites.

**Figure 13.** (a) Master curve of $G'$ and $G''$ at the reference temperature ($T_{ref}$ = 170 °C) for SAN, (b) $\ln\alpha_T$ as a function of $1/T$ for SAN.

**Table 1.** Interfacial tension and wetting coefficient calculated by using the harmonic mean equation

| Temperature (°C) | Interfacial tension (mN/m) | | | wetting coefficient ($\omega_a$) | Location predication |
|---|---|---|---|---|---|
| | $\gamma_{PMMA-MWNT}$ | $\gamma_{SAN-MWNT}$ | $\gamma_{PMMA-SAN}$ | | |
| 170 | 10.04 | 5.02 | 1.56 | 3.23 | SAN |
| 180 | 10.05 | 5.01 | 1.54 | 3.28 | SAN |
| 190 | 10.08 | 5.02 | 1.52 | 3.33 | SAN |
| 200 | 10.13 | 5.03 | 1.51 | 3.38 | SAN |

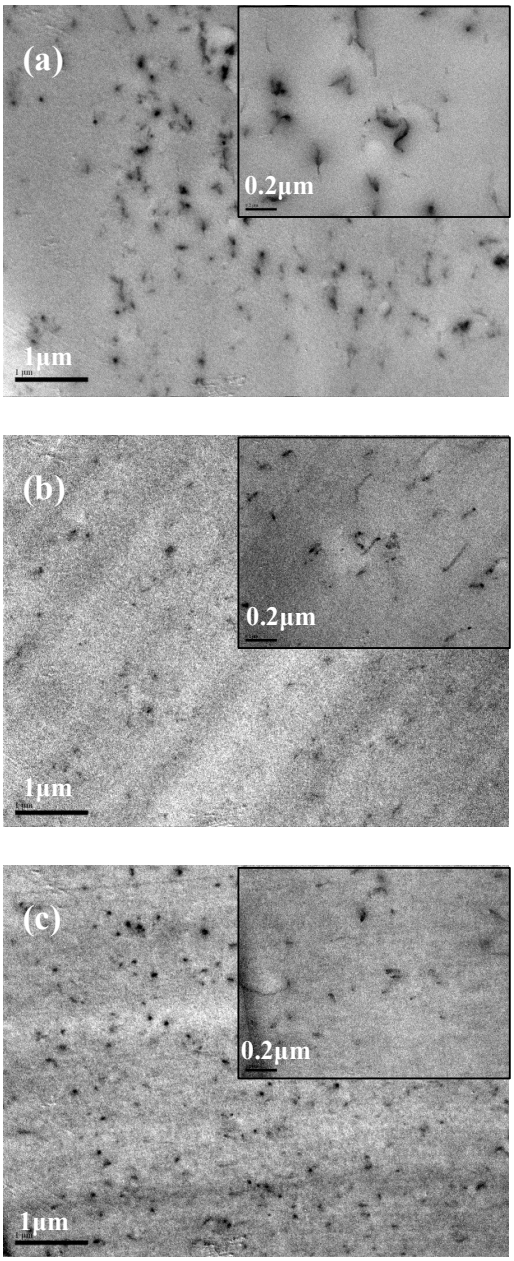


**Figure 1.** TEM micrographs of (a) PMMA/MWNT (100/0.2), (b) SAN/MWNT (100/0.2) and (c) PMMA/SAN/MWNT (57/43/0.2) nanocomposites without annealing.

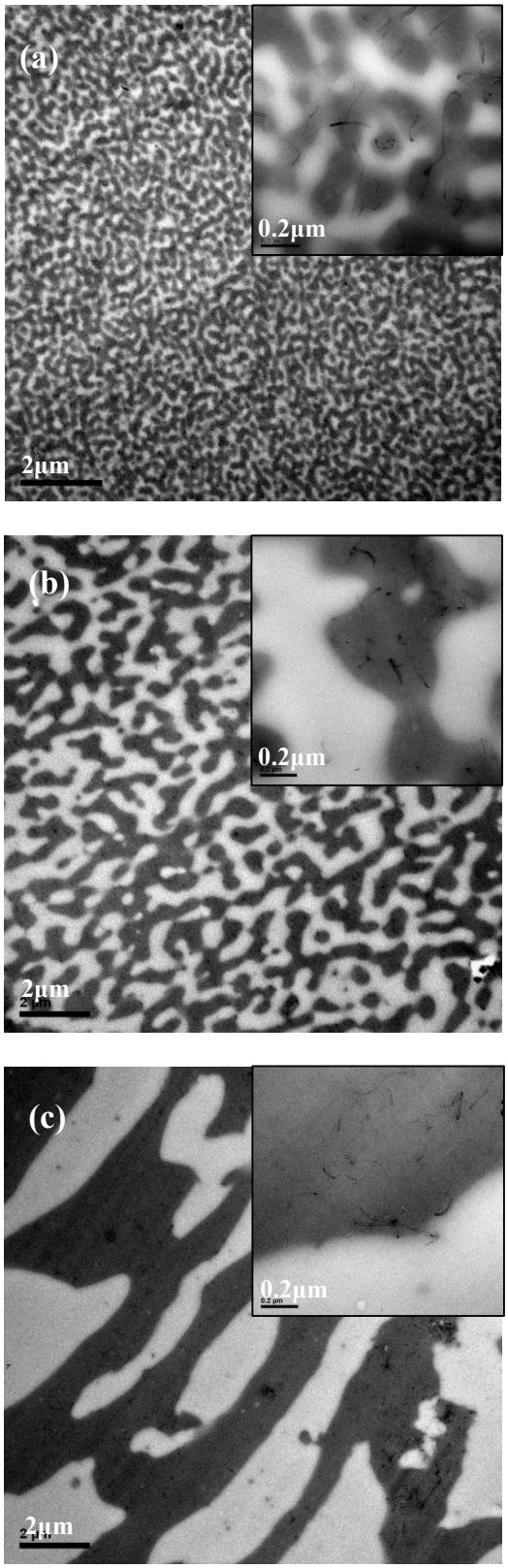


**Figure 2.** TEM micrographs of PMMA/SAN/MWNT (57/43/0.4) nanocomposites annealed at 180 $^{o}$C for (a) 100 s, (b) 1000 s and (c) 4 h.

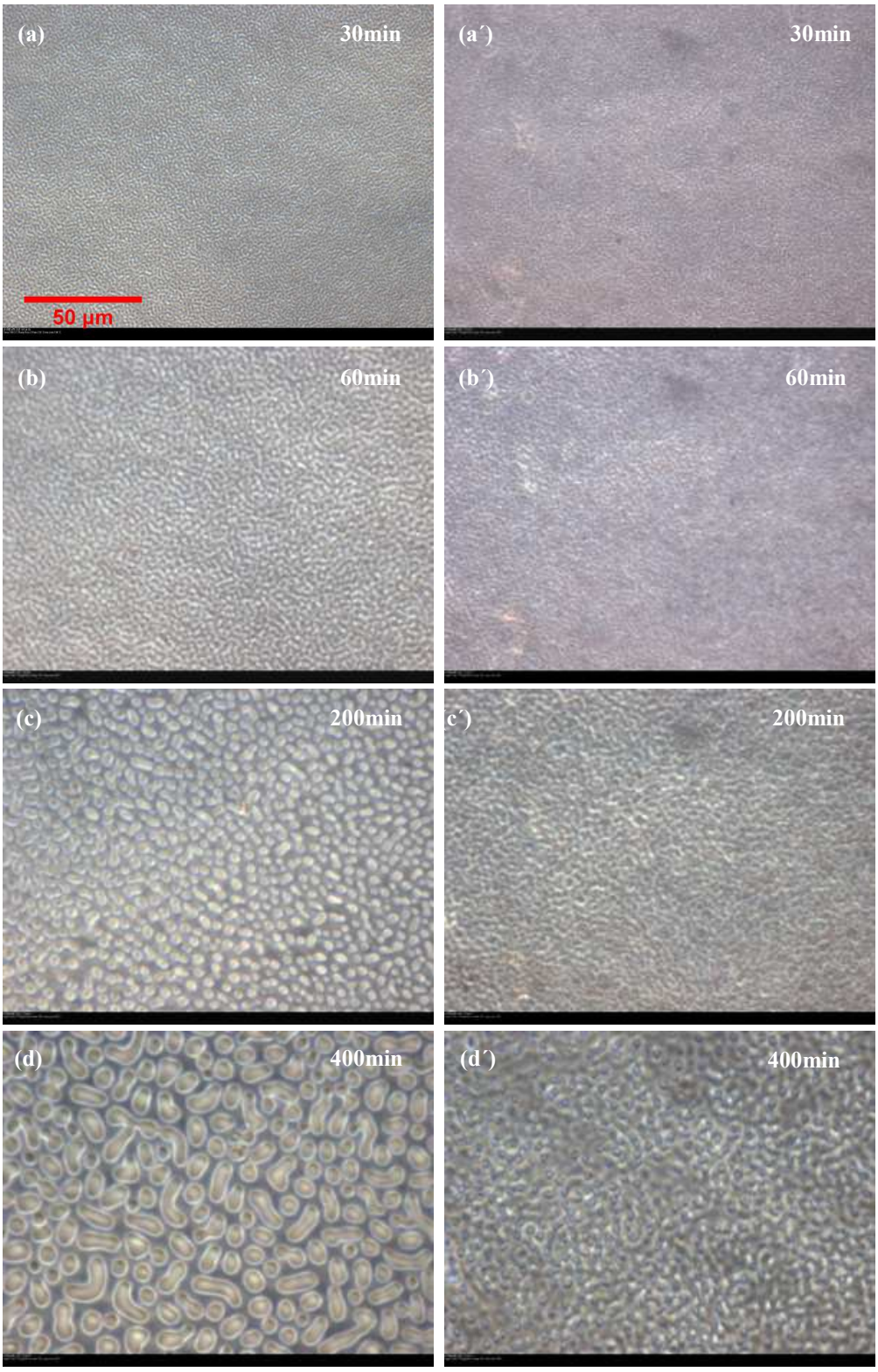


**Figure 3.** Morphology evolution of (a) (b) (c) (d) PMMA/SAN (57/43) blend and (a´) (b´) (c´) (d´) PMMA/SAN/MWNT (57/43/0.2) nanocomposite under annealing at 190 $^{o}$C for different time.

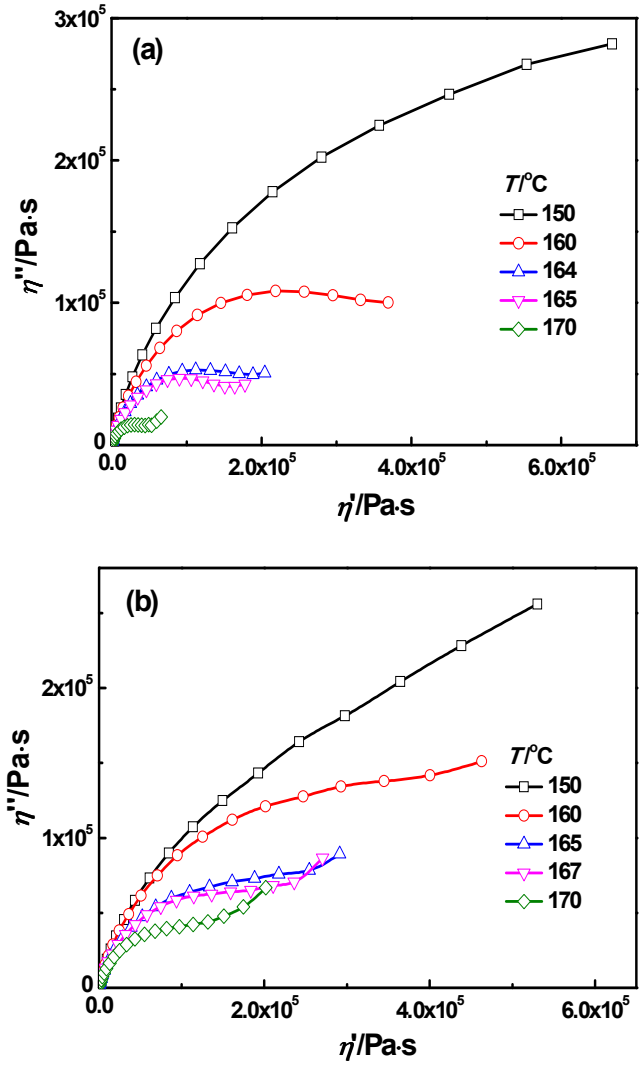


**Figure 4.** Cole-Cole plots of (a) PMMA/SAN (57/43) blend and (b) PMMA/SAN/MWNT (57/43/0.2) nanocomposite at different temperatures.

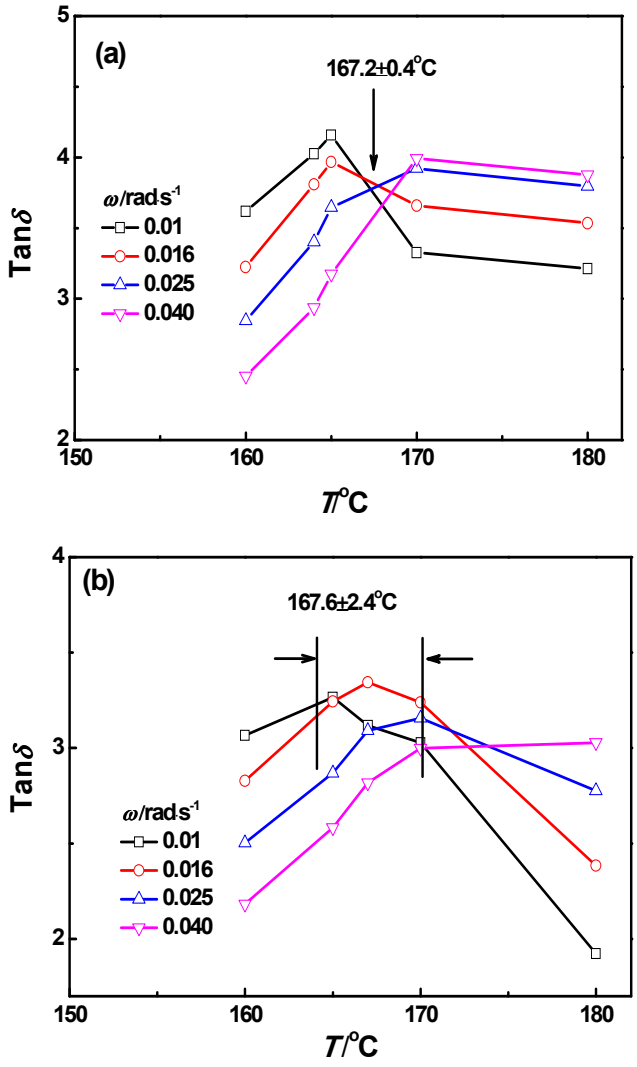


**Figure 5.** Temperature dependence of tan $\delta$ under different frequencies (0.01~0.040rad·s$^{-1}$) for (a) PMMA/SAN (57/43) blend and (b) PMMA/SAN/MWNT (57/43/0.2) nanocomposite.

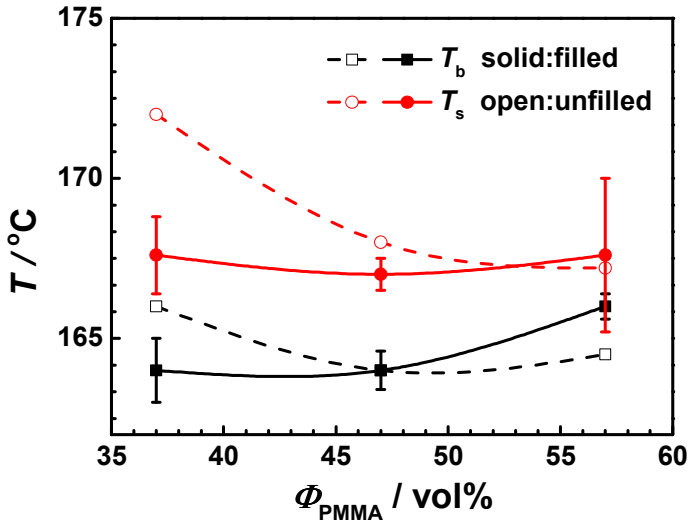


**Figure 6.** Apparent phase diagram of PMMA/SAN blends and 0.2 vol% MWNT filled PMMA/SAN nanocomposites.

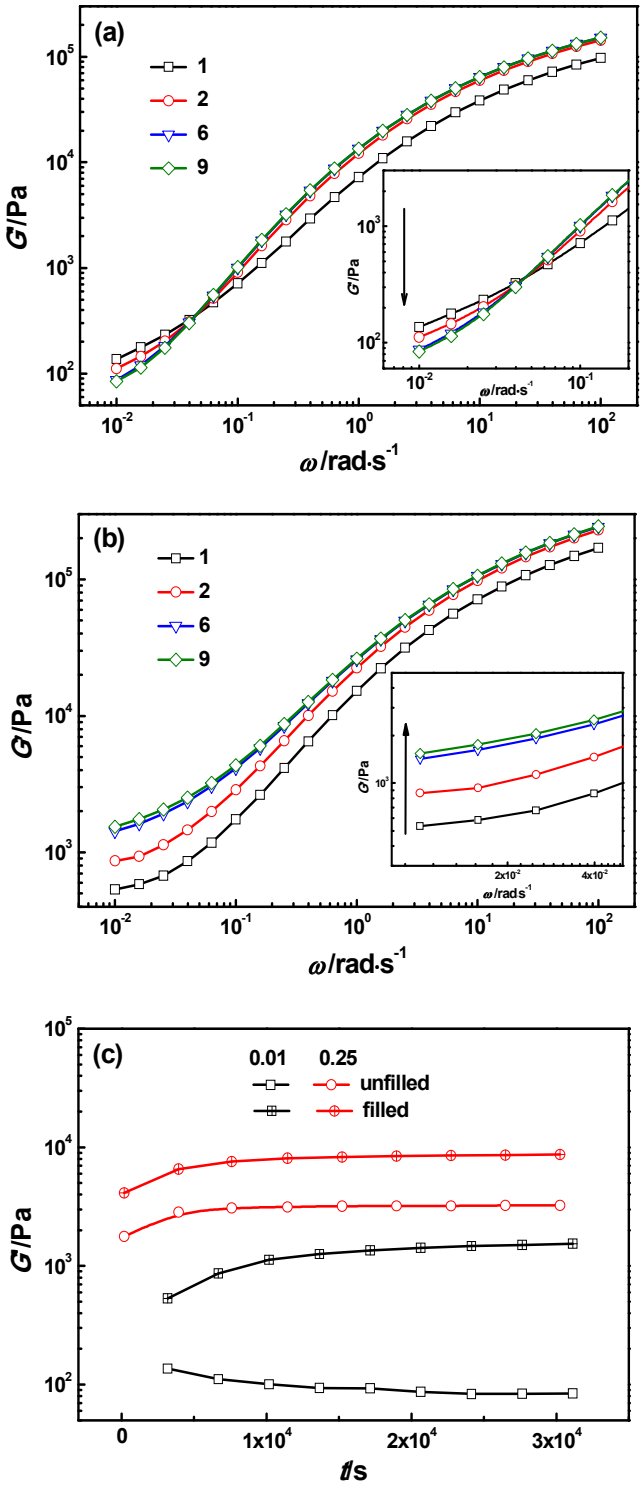


**Figure 7.** Dynamic storage modulus ($G'$) under cyclic frequency sweeps at 180 °C for (a) PMMA/SAN (57/43) blends and (b) PMMA/SAN/MWNT (57/43/0.2) nanocomposites; (c) $G'$ for the unfilled and filled systems as a function of time ($t$) at 180 °C at 0.25 rad·s$^{-1}$ and 0.01 rad·s$^{-1}$.

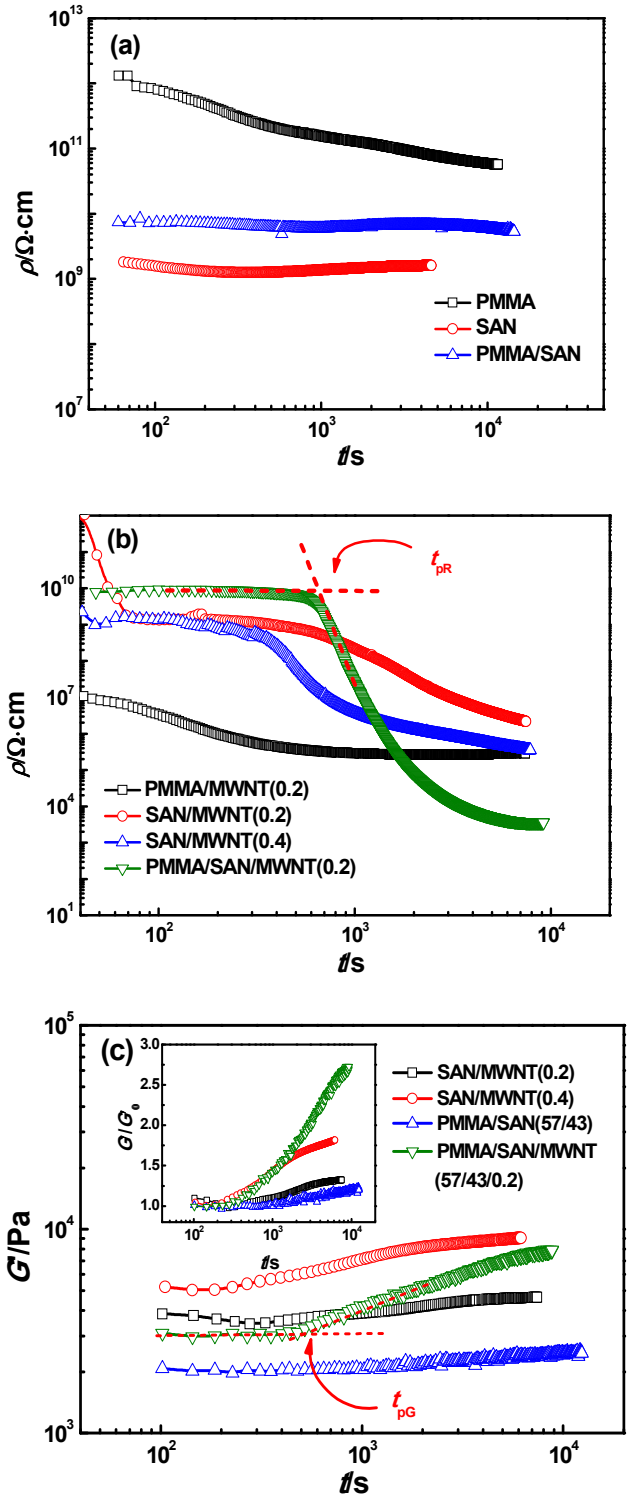


**Figure 8.** Time evolution of volume resistivity $\rho$ for (a) unfilled PMMA,SAN, PMMA/SAN (57/43) systems, (b) MWNT filled PMMA, SAN, PMMA/SAN (57/43) nanocomposites; (c) time evolution of dynamic storage modulus $G'$ at 180 °C. The insert plot shows the normalized dynamic modulus $G'/G'_0$ at 180 °C.

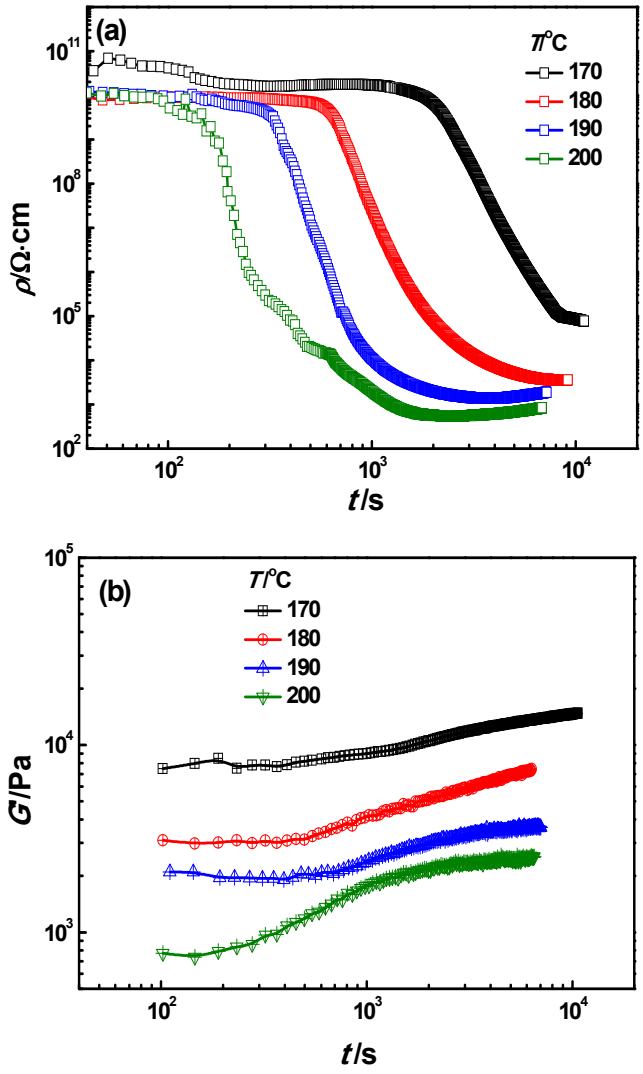


**Figure 9.** Time evolution of (a) $\rho$ and (b) $G'$ for PMMA/SAN/MWNT (57/43/0.2) nanocomposites at different annealing temperatures.

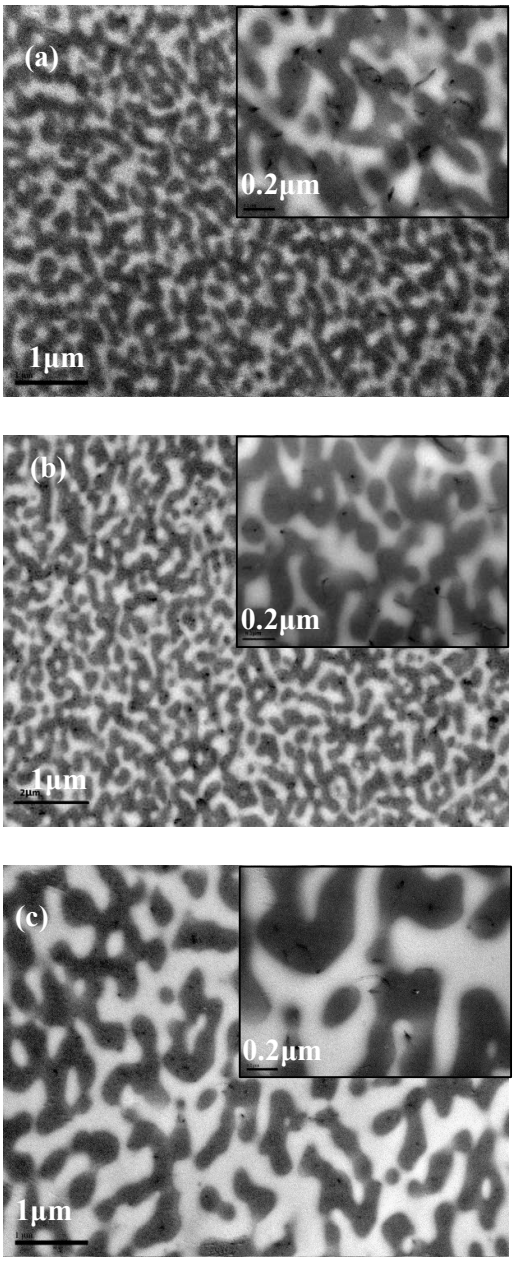


**Figure 10.** TEM micrographs of PMMA/SAN/MWNT (57/43/0.2) nanocomposites annealed at (a) 170 $^{o}$C for 500 s, (b) 180 $^{o}$C for 300 s and (c) 190 $^{o}$C for 200 s.

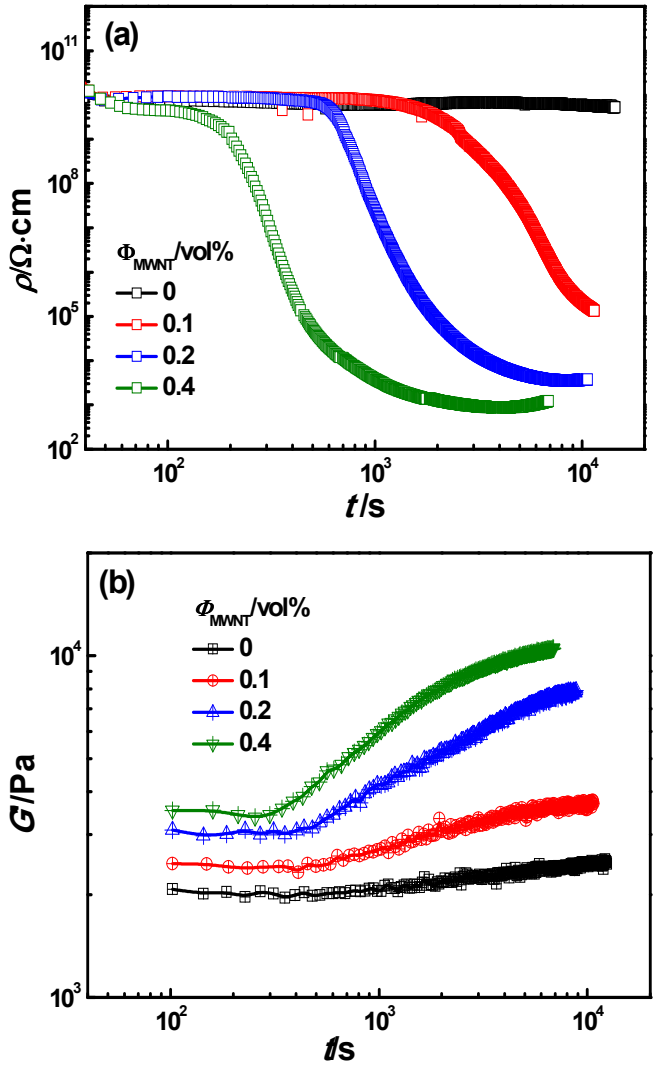


**Figure 11.** Time evolution of (a) $\rho$ and (b) $G'$ for PMMA/SAN/MWNT (57/43/x) nanocomposites with different MWNT volume fractions $\phi$ at 180 °C.

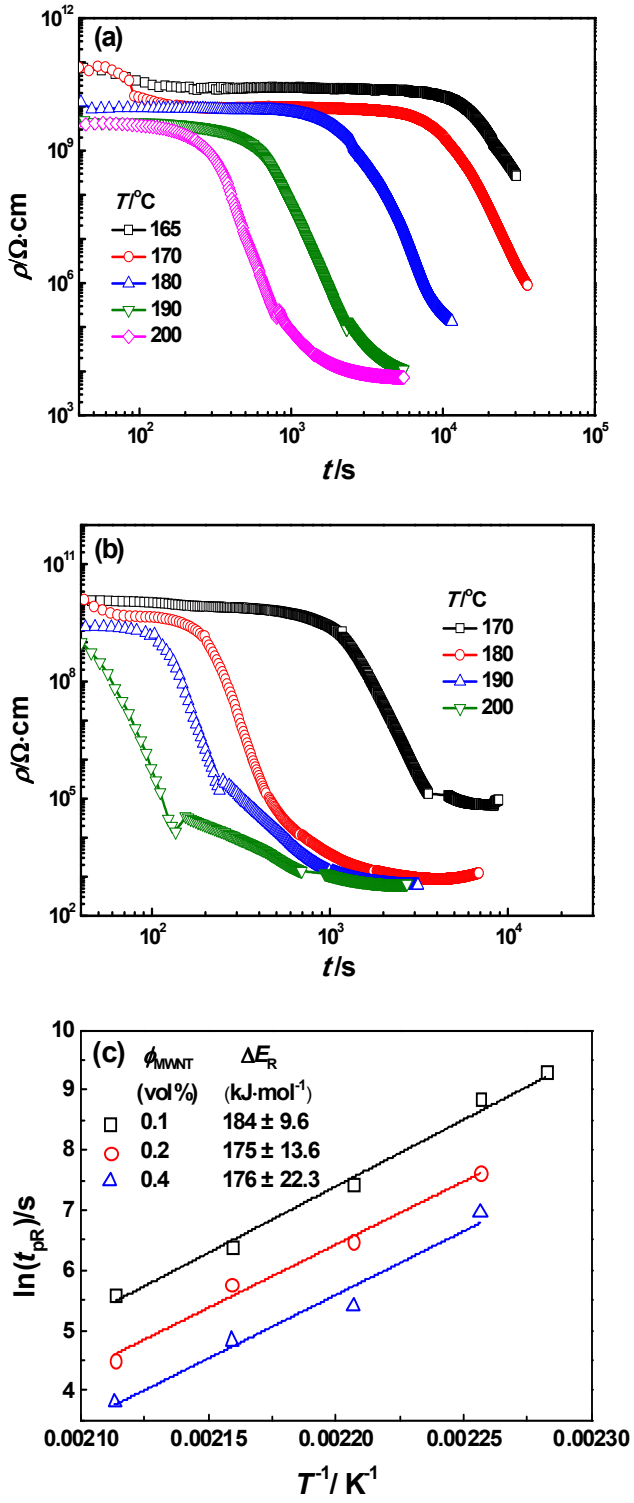


**Figure 12.** Time evolution of $\rho$ for (a) PMMA/SAN/MWNT (57/43/0.1) and (b) PMMA/SAN/MWNT (57/43/0.4) nanocomposites at different annealing temperatures. (c) $\ln t_{pR}$ as a function of $1/T$ for MWNT filled PMMA/SAN (57/43) nanocomposites.

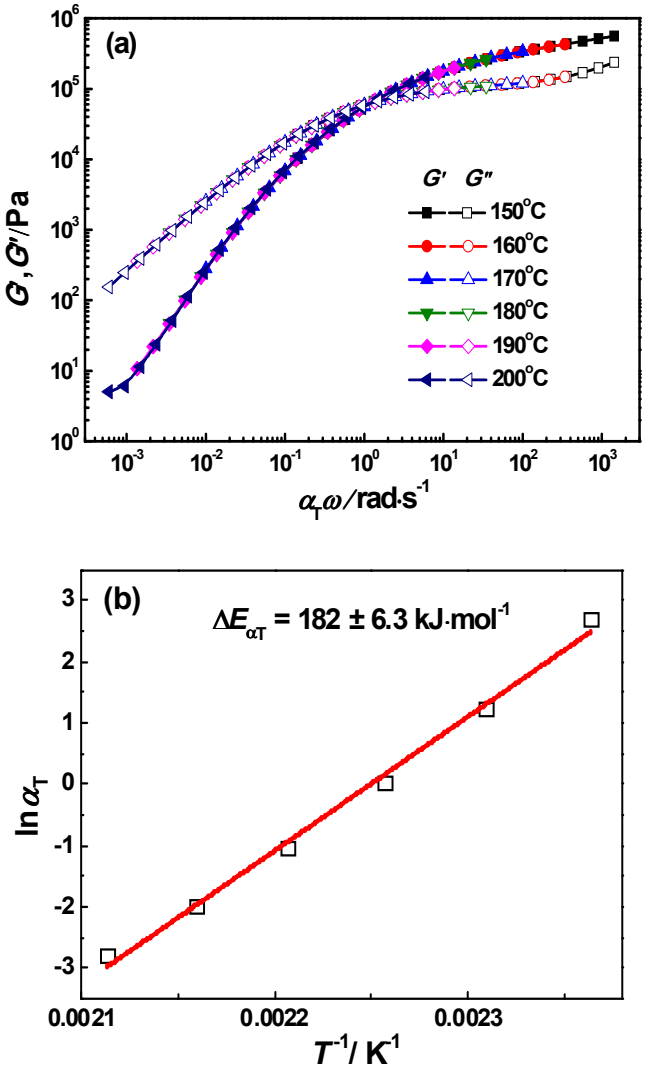


**Figure 13.** (a) Master curve of $G'$ and $G''$ at the reference temperature ($T_{ref}$ = 170 °C) for SAN, (b) $\ln\alpha_T$ as a function of $1/T$ for SAN.

MWNTs migrate and aggregate in SAN-rich phase to form the double percolated structure with thermal-induced phase separation of blend matrix.